



PAPER

Conductive gelatin methacrylate-poly(aniline) hydrogel for cell encapsulation

To cite this article: Stephen W Sawyer *et al* 2018 *Biomed. Phys. Eng. Express* **4** 015005

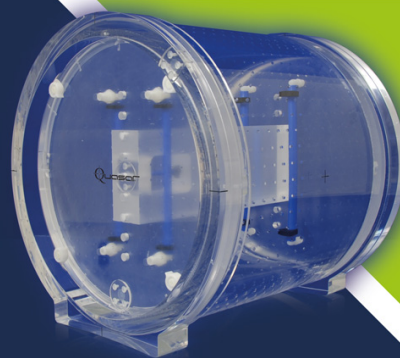
View the [article online](#) for updates and enhancements.

Related content

- [A fast-degrading thiol-acrylate based hydrogel for cranial regeneration](#)
A M Emmakah, H E Arman, J C Bragg *et al.*
- [3D bioprinting of GelMA scaffolds triggers mineral deposition by primary human osteoblasts](#)
Christine McBeth, Jasmin Lauer, Michael Ottersbach *et al.*
- [A bioprintable form of chitosan hydrogel for bone tissue engineering](#)
Turul Tolga Demirta, Gülseren Irmak and Meneme Gümüdereliolu

Quantify 3D Geometric Distortion in MR Images

Verify the accuracy of target delineation and treatment efficacy for MRgRT



Watch Video

modusQA

Accuracy. Confidence.™



PAPER

Conductive gelatin methacrylate-poly(aniline) hydrogel for cell encapsulation

RECEIVED
12 September 2017REVISED
27 September 2017ACCEPTED FOR PUBLICATION
9 October 2017PUBLISHED
27 November 2017Stephen W Sawyer^{1,3}, Ping Dong^{1,3}, Sarah Venn¹, Andrew Ramos¹, David Quinn¹, Jason A Horton² and Pranav Soman¹ ¹ Department of Biomedical and Chemical Engineering, Syracuse University, Syracuse, NY, United States of America² Department of Orthopedic Surgery, SUNY Upstate Medical University, Syracuse, NY, United States of America³ co-first authors.E-mail: psoman@syr.edu

Keywords: polyaniline, gelatin methacrylate, cell encapsulation, stereolithography

Abstract

New conductive hydrogels with superior biocompatibility continue to be developed in order to serve as bioactive scaffolds capable of modulating cellular functionality for tissue engineering applications. We developed an electrically conductive gelatin methacrylate-poly(aniline) (GelMA-PANi) hydrogel that is permissive of matrix mineralization by encapsulated osteoblast-like cells. Incorporation of PANi clusters within the GelMA matrix increases the electro-conductivity of the composite gel, while maintaining the osteoid-like soft mechanical properties that allows three-dimensional encapsulation of living cells. Viability of human osteogenic cells encapsulated within GelMA-PANi hydrogels was similar to that of GelMA. Cells within GelMA-PANi also demonstrated the capability of depositing mineral within the hydrogel matrix after being chemically induced for two weeks, although the total mineral content was lower as compared to GelMA. Additionally, we demonstrated that the GelMA-PANi-composite hydrogel could be printed in complex, user-defined geometries using digital projection stereolithography.

Introduction

The past few decades have seen the development of new biomaterials capable of mimicking the *in vivo* 3D microenvironment in an effort to modulate cellular responses for a variety of tissue engineering applications. To this end, hydrogels have emerged as ideal biomaterials in the development of biomimetic 3D tissue scaffolds due to their hydrated extra-cellular matrix like properties [1–3]. Within the past few years, hydrogel biomaterials laden with living cells have also been used to simulate the 3D *in vivo* microenvironment as an alternative to conventional 2D configurations [4, 5]. However, the electrically non-conductive nature of hydrogels impedes its use for excitable cells such as neural, skeletal and cardiac muscle, and bone cells [6, 7]. To extend the utility of hydrogels, conducting elements like metallic nanoparticles [8–14] and inherently conductive polymers (IHPs) [6, 15–19] have been incorporated within hydrogel matrices in order to add conductive properties to the 3D microenvironments.

Most recently hydrogels have been combined with polyaniline (PANi), a commonly used IHP [17, 20], since it is capable of conducting electricity due to the presence of conjugated double bonds in its chemical structure [6]. Additionally, PANi has favorable properties to researchers such as low cost, ease of synthesis, and the ability to electrically switch between resistive and conductive states. Studies involving PANi have been extensively centered around the seeding of cells on pre-fabricated PANi films, as synthesis of 2D thin films can be processed quite easily with current manufacturing methods such as inkjet printing, casting, self-assembly, and electrospinning [21–25]. The use of PANi in engineering cell-laden three-dimensional biomimetic constructs has been limited due to its difficult and non-biocompatible processing steps and its insolubility in common solvents [17, 26–28].

Previously, we have reported that PANi can be integrated with synthetic PEGDA and naturally derived gelatin methacrylate (GelMA) hydrogels *in situ* in order to develop 3D conductive-hydrogels that are sufficiently biocompatible with seeded cells

[29, 30]. However, like studies similar to ours, the harsh processing methods were incompatible with cell encapsulation approaches. In this study, we developed a conductive PANi-GelMA composite by incorporating PANi clusters within a photo-polymerizable GelMA hydrogel and investigate the ability of encapsulated osteoblast-like cells to mineralize within the hydrogel matrix. Additionally, we provide a proof-of-concept that our conductive hydrogel can be printed using digital stereolithography in order to create defined areas of mineralization.

Materials and methods

Gelatin methacrylate/poly(aniline) solution preparation

Poly(aniline) clusters (PANi) were synthesized according to published studies [31–33]. Briefly, aniline (Acros Organics) and ammonium persulfate (APS, Sigma Aldrich) were dissolved separately in 1 M hydrochloric acid (HCl) to specified concentrations of 0.32 M and 0.16 M, respectively. Once dissolved, the two solutions were quickly mixed and left to stand for 24 h (figure 1(A)). After polymerizing, the aniline-APS polymer solution was dialyzed against distilled water in 12–14 kDa dialysis tubing (Spectrum™, Thermo Fisher Scientific) for 3 d. After 72 h, the dialyzed solution was filtered with a micro-filter paper (pore size-0.46 μm) and dried at room temperature.

Gelatin methacrylate (GelMA) macromer was synthesized according to our published work [34]. Briefly, porcine skin gelatin (Sigma Aldrich) was mixed at 10% (w/v) in phosphate buffered saline (PBS, Thermo Fisher Scientific), combined with methacrylic anhydride, dialyzed against distilled water, lyophilized, and stored at -80°C until needed. GelMA pre-polymer solution was created by combining the freeze-dried GelMA macromer with PBS and 0.25% UV photoinitiator Irgacure 2959 (Specialty Chemicals) in specific ratios depending on the desired application (% w/v).

PANi was dissolved in 0.1 M HCL in order to produce solutions of 1%, 5%, 7.5%, 10%, and 15% (w/v), respectively, and sonicated for 30 min prior to incorporation into GelMA to facilitate dispersion. After sonication, PANi solution was added to 15% (w/v) GelMA pre-polymer solution to create the hybrid GelMA-PANi solutions used for mechanical analysis (referred to as 0.05, 0.25, 0.375, 0.5, and 0.75 PANi respectively).

Characterization of hybrid conductive hydrogel

The size and morphology of the PANi clusters were analyzed via transmission electron microscopy (TEM, JOEL 2000EX) under an acceleration voltage of 100 kV. As previously described, a 0.1% PANi solution was synthesized and deposited onto a thin bar formvar-carbon hexagonal 400 Cu mesh grid

(FCFTH400-Cu, Electron Microscopy Sciences) and subsequently dried in a desiccant chamber. After drying, the grids were stained with a 2% uranyl acetate solution and placed in the desiccant chamber briefly prior to imaging.

In order to show incorporation of PANi into GelMA hydrogel solution, the UV-visible absorption spectra for uncured 15% (w/v) GelMA, 0.1% PANi solution, and combined GelMA-PANi pre-polymer solution was obtained using a UV-Visible Spectrophotometer (Evolution 201, Thermo Fisher Scientific). To obtain the measurements, 3 ml of each sample solution was added to a plastic cuvette standard to the device. Absorbance at wavelengths between 200 and 800 nm was recorded, and data was exported to Excel (Microsoft) for analysis. Background calculations were normalized to deionized water.

Hydrogel slabs used for mechanical, electrical, and swelling measurements were made by injecting the GelMA-PANi solutions between two glass slides separated by Teflon spacers (0.81 mm thick for electrical characterization; 1.62 mm thick for mechanical and swelling characterization). The pre-polymer solution was crosslinked via UV light (Omnicure S2000 UV Lamp, Lumen Dynamics) for 10 min (UV intensity 10 W cm^{-2}) to generate samples.

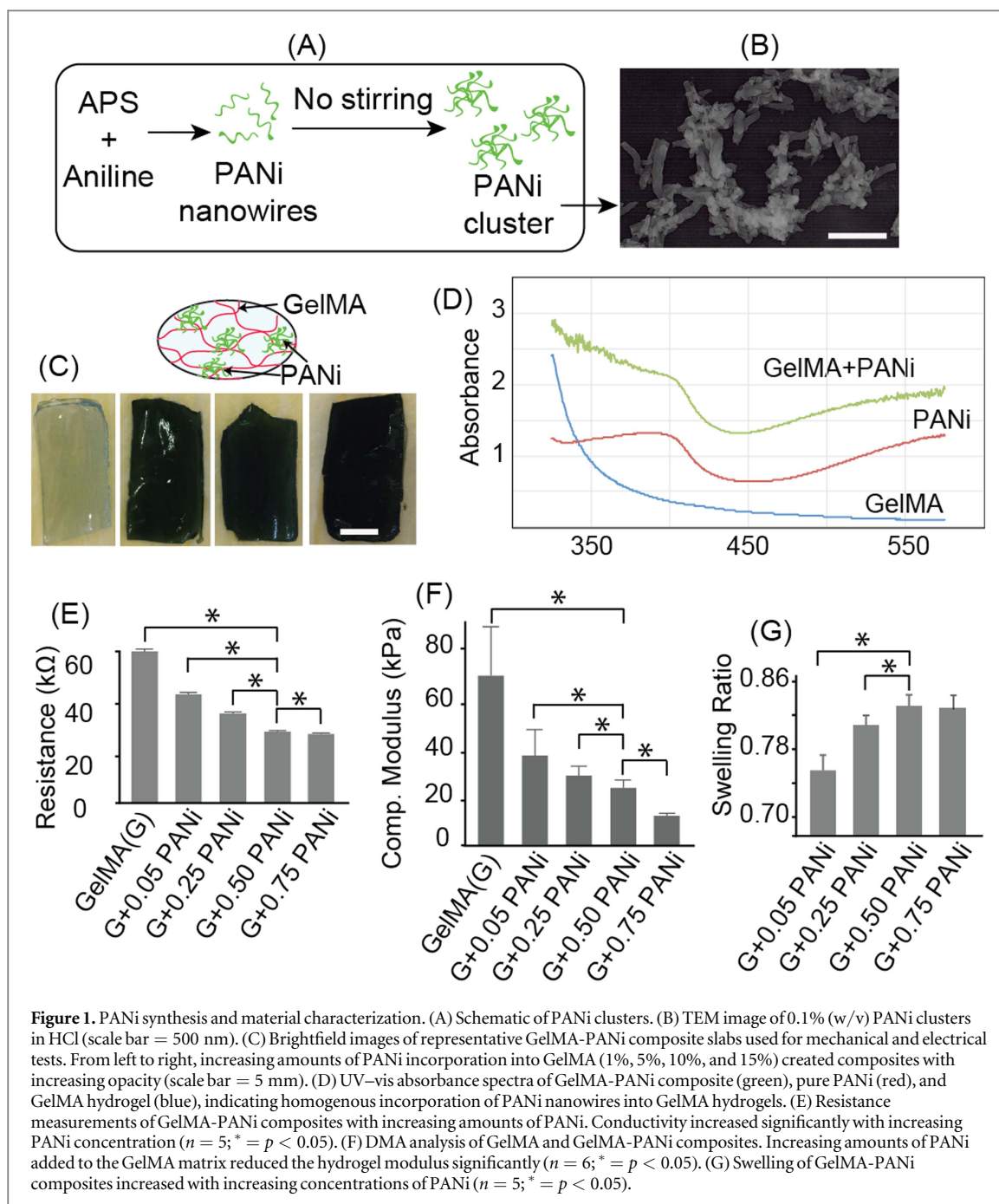
The electrical conductivity of GelMA-PANi slabs were measured against 15% (w/v) GelMA using a custom made electrical chip. 0.81 mm slabs were made as previously described, placed inside the chip, and subsequently compressed with a 10 g weight. Resistances were measured incrementally from 0 to 300 s and the data points between 100 and 200 s were averaged for the reported resistance values.

The compressive modulus of both the GelMA and GelMA-PANi slabs were measured via dynamic mechanical analysis (DMA, Q800, TA Instruments, Inc.). A 15% (w/v) GelMA slab with a thickness of 1.62 mm was compared against 15% (w/v) GelMA-PANi slabs of the same thickness containing four different concentrations of stock PANi solution (1%, 5%, 10%, and 15%). A new slab was created prior to each test and was placed on a compression clamp where the strain was incrementally increased from 5% to 20% with a preloaded force of 0.01 N.

The swelling ratios of the four different types of GelMA-PANi slabs were calculated by the following equation:

$$\text{swelling ratio (\%)} = (W_w - W_d) / W_d * 100\%,$$

where W_w is wet weight and W_d is dry weight. To obtain the measurements, fresh GelMA-PANi slabs were immersed in deionized water for 3 d, weighed, dried under ambient humidity for 7 d at room temperature, and weighed again.



Saos-2 culture and encapsulation

Human osteosarcoma cells (Saos-2, ATCC) were employed as analogs for osteoblasts as they are generally representative of the early stages of osteogenic differentiation and mineralization [35]. The Saos-2 cells were cultured in Dulbecco's Modification of Eagles's Media (DMEM, Life Technologies) supplemented with 1% GlutaMAX (G, Life Technologies), 1% penicillin-streptomycin (Life Technologies) and 10% fetal bovine serum (FBS lot G12102, Atlanta Biologicals), and cultivated at 37 °C in a humidified 95%air/5% CO₂ atmosphere. Cells were grown to confluence and passaged using 0.25% trypsin-EDTA (Life Technologies) prior to any new experiment.

Saos-2 cells were encapsulated in GelMA or GelMA-PANi by mixing 5 μ l of a cell suspension containing approximately 10 000 cells μ l⁻¹ with 15 μ l of either 20% (w/v) GelMA or 20% (w/v) GelMA supplemented with PANi (refer to G + 0.5PANi in figure 1). The 20 μ l cell/hydrogel pre-polymer solution was pipetted into 5 mL of autoclaved vegetable oil, taking advantage of a surface tension technique used in previous studies [34] and UV cured for 1 min and 20 s using a Hamamatsu LED Controller (Hamamatsu C11924-511; Hamamatsu Photonics K.K., Japan) with an output of 5 mW cm⁻². Once cured, the GelMA and GelMA-PANi beads containing approximately 50 000 cells were washed in sterile PBS and

transferred into cell culture media. Media was refreshed every 2–3 d on each construct using standard cell culture procedures.

Cellular viability and morphology

After 1 d of culture under standard conditions, GelMA and GelMA-PANi samples containing encapsulated Saos-2 cells were analyzed for viability using a standard Live/Dead assay. This time point was chosen to account for process-associated apoptosis and necrosis which can take several hours to execute. To measure viability, GelMA and GelMA-PANi constructs were transferred into warmed media supplemented with calcein-AM (1:2000 dilution, Life Technologies) and ethidium homodimer (1:500 dilution, Life Technologies), and incubated for 1 h prior to imaging, respectively staining live cells green and dead cells red. Live/Dead images were taken at the top, middle, and bottom of each sample using a Leica DMI4000 B inverted research microscope (Leica) and the relative proportion of live and dead cells were analyzed using ImageJ software (NIH).

GelMA and GelMA-PANi samples to be imaged for nuclei and f-actin were fixed in cold 4% paraformaldehyde (Sigma-Aldrich) after 3 d of culture and were subsequently transferred into room temperature PBS for staining. Samples were treated with 0.2% Triton X-100 (Sigma) for 30 min, washed twice with PBS, and stained for actin with Alexa Fluor 488 Phalloidin (1:100 dilution, Life Technologies). Sample nuclei were counterstained with $2.5 \mu\text{g ml}^{-1}$ 4,6-diamidino-2-phenylindole (DAPI, 1:50 dilution, Life Technologies) and imaged with a LSM 780 laser scanning confocal microscope (Zeiss).

Mineralization

After 1 d of culture, GelMA and GelMA-PANi hydrogels containing approximately 50 000 encapsulated Saos-2 cells were chemically stimulated to induce mineral deposition. Specifically, the hydrogel samples were transferred 24 h after encapsulation into an osteogenic medium consisting of DMEM, 10% FBS, 1% PSG, 10 nM dexamethasone (DEX, Sigma-Aldrich), 100 μM L-ascorbic acid-2-phosphate (AA2P, Sigma-Aldrich), and 10 mM β -glycerophosphate (BGP, Sigma-Aldrich). Osteogenic media was refreshed every 2–3 d on each construct using standard cell culture procedures.

After 14 d of culture in osteogenic media, GelMA and GelMA-PANi samples were fixed in cold 4% formaldehyde for 24 h, after which they were washed and stored in PBS. Samples were imaged for mineral content at a $16 \mu\text{m}^3$ voxel resolution using a μCT -40 instrument operating at 55kVp with a 200 ms integration time (Scanco Medical AG, Brüttsellen, Switzerland) [36]. Samples were lightly packed in PBS saturated cotton gauze inside standard μCT sample tubes. After imaging, samples were transferred into PBS and prepared for histological analysis.

RT-qPCR

RT-qPCR was performed on RNA extracts from GelMA and GelMA-PANi samples to evaluate expression of a panel of osteogenic genes. For RNA extraction, GelMA and GelMA-PANi samples were created in triplicate, grown in culture medium for either 1 or 14 d, washed in PBS, and transferred to stock cell lysis buffer that is supplied by Qiagen RNeasy Mini Kits (Qiagen). Sample triplicates were homogenized in the buffer three times via a Precellys homogenizer (Bertin Instruments), transferred to a Qiagen Qiashredder column, and subsequently processed via published Qiagen RNeasy protocols. Extracted RNA was checked for quantity and purity by UV absorbance spectrometry using a Tecan Infinite 200 Nanoquant plate reader (Tecan Trading AG), and stored at -80°C until needed.

After RNA extraction, cDNA was created according to published protocol with an iScript Reverse Transcription kit (Bio-Rad Laboratories, Inc.) in an Eppendorf Mastercycler pro (Eppendorf AG) for qPCR reactions. iTaq universal SYBR Green Supermix (Bio-Rad Laboratories, Inc.) was used for the real time qPCR reaction according to manufacturer recommended protocol in an Eppendorf RealPlex 2 Mastercycler (Eppendorf AG). Relative expression of five different transcripts associated with osteogenesis were compared by real time RT-qPCR and normalized to human beta actin (ACTB) expression: osteonectin (SPARC), osteopontin (SPP1/OPN), osteocalcin (BGLAP), human collagen 1 alpha 1 (hCOL1A1), and human alkaline phosphatase (hALPL). Oligonucleotide primers were synthesized by RealTimePrimers (ACTB, SPARC, SPP1/OPN, BGLAP) or Eurofins Scientific (hCOL1A1 and hALPL). Amplicons were evaluated for primer specificity by melt-curve analysis and agarose gel electrophoresis. Amplification efficiency for each primer pair was determined by interpolation to an 8-point standard curve of two-fold dilutions of cDNA.

Histological analysis

GelMA and GelMA-PANi samples were prepared for histological analysis via standard paraffin embedding protocols. Briefly, samples containing encapsulated cells were grown in culture medium for either 1 d (no chemical induction) or 14 d (with chemical induction) and fixed in cold 4% paraformaldehyde for 24 h before dehydration through ascending ethanol series, clearing in xylene, and infiltration and embedment in Type 9 paraffin at 58°C . Sections (5 μm thick) were cut on a rotary microtome (RM2155, Leica) and mounted on SuperFrost Plus slides.

Hematoxylin and eosin (H&E) staining

Sections were deparaffinized in xylene and rehydrated through descending ethanol series to deionized water and stained by standard H&E procedure using Mayer's

Hematoxylin and Eosin/Phloxine solutions (Electron Microscopy Sciences). Sections were then dehydrated through an ethanol series, cleared in xylene, and cover-slipped with Permount (Fisher Scientific).

Collagen 1- α -1 immunohistochemistry

For immunohistochemical demonstration of *de novo* collagen synthesis, sections of GelMA or GelMA-PANi samples were de-paraffinized and rehydrated as described above. Prior to immunohistochemical staining, heat-induced epitope retrieval was performed in 10 mM citrate buffer (pH 6.0) for 4 min using a pressure cooker. Sections were subsequently blocked with 2.5% horse serum for 1 h (ImmPRESS™ VR Reagent Kit, Vector Laboratories) and afterwards incubated with 2 $\mu\text{g ml}^{-1}$ of mouse anti-collagen type 1 aminopropeptide IgG (SP1.D8, Developmental Studies Hybridoma Bank) diluted in blocking buffer for 16 h at 4 °C. Slides were then washed several times in PBS, and endogenous peroxidase activity was inactivated by incubation in blocking solution (Bloxall, Vector Laboratories) for 10 min at room temperature. Next, sample slides were rinsed with PBS and probed for primary immunoreactivity using a peroxidase-conjugated horse anti-mouse secondary antibody (Anti-Mouse IgG Peroxidase, ImmPRESS™ VR Reagent Kit, Vector). After 20 min, the slides were rinsed with PBS and sections were probed for 10 min using a polymeric peroxidase substrate (ImmPACT Chromogen, ImmPACT™ DAB Peroxidase Substrate Kit, Vector), washed in deionized water, and counterstained with Hematoxylin. Sections were then dehydrated through ethanol, cleared in xylene, and cover-slipped with Permount.

Alizarin Red S and toluidine blue staining (mineral and counterstain)

Alizarin Red S was used to visualize calcium mineral deposition in the GelMA and GelMA-PANi samples. Briefly, sections were deparaffinized in xylene and rehydrated through ethanol to deionized water, then incubated in 40 mM Alizarin Red S solution (4.1 pH, Sigma) for approximately 5 min. Slides were then washed in deionized water and counterstained with Toluidine blue O (Sigma) for 2 min. Sections were then dehydrated through ethanol, cleared in xylene, and cover-slipped with Permount.

Histological imaging

Cover-slipped and stained sections were imaged using a Nikon Eclipse E-400 microscope (Nikon Corporation).

Printing GelMA-PANi-cells using digital stereolithography

A UV-stereolithography platform with a digital micro-mirror device (DMD) was used to print GelMA-PANi lines containing encapsulated Saos-2 cells. A 20 μl solution of 15% GelMA-PANi containing 50 000 cells

was created as previously described and pipetted drop wise onto a standard glass slide. Two glass spacers with thicknesses of 1 mm were fixed onto the glass slide, thereby creating a 'well' in which the GelMA-PANi cell solution was contained. A methacrylated 12 mm cover slip (Platinum Line) was placed on top of the spacers. Ultraviolet light from an Omnicure S2000 was focused onto the samples via a digital mirror array preprogrammed with a 'cross-shaped' digital mask for 4.7 s (UV intensity 10 W cm^{-2}). The coverslip was then washed with 37 °C PBS to remove uncured GelMA-PANi, and immediately transferred into culture media. Live/dead staining was performed on the 3D printed structure as previously described at 24 h post encapsulation. 3D printed samples were also subjected to osteogenic media as previously described for two weeks prior to μCT analysis.

Statistical analysis

Numerical data was entered into Microsoft Excel to calculate mean and standard deviation and perform Student's T-test to assess statistical significance of differences; *p*-values less than 0.05 were accepted as statistically significant.

Results

Poly(aniline) synthesis and material characterization

Past work on conductive hydrogels has focused on adding conductive properties to the hydrogel matrices during the initial synthesis process. Unfortunately, the harsh nature of the synthesis creates environments unsuitable for cellular encapsulation *in situ* and, as a result, inhibits these composites from being used for subsequent tissue engineering applications. In order to work around this issue, PANi clusters were synthesized independently of the GelMA macromer and added in various concentrations directly prior to hydrogel curing and cellular encapsulation (figure 1(A)). Upon polymerization, the poly(aniline) solution was dialyzed against distilled water and lyophilized to create PANi clusters (referred to as simply PANi in this work). Transmission electron microscopy images of 0.1% (w/v) PANi in HCl are representative of the PANi synthesized by our method (figure 1(B)). For electrical and mechanical studies, 1%, 5%, 10%, and 15% (w/v) stock PANi solutions in HCl were added to GelMA pre-polymer solutions to create hybrid GelMA-PANi hydrogels exhibiting an increasing opacity (figure 1(C)). In order to show that low concentrations of PANi could be incorporated homogeneously within the GelMA matrix, 0.1% (w/v) PANi was combined with GelMA pre-polymer solution and subjected to UV-vis spectroscopy (figure 1(D)). As indicated by the absorbance spectra, GelMA-PANi hybrid solutions exhibited the characteristic spectra associated with pure PANi in HCl. While PANi incorporation into the GelMA matrix was

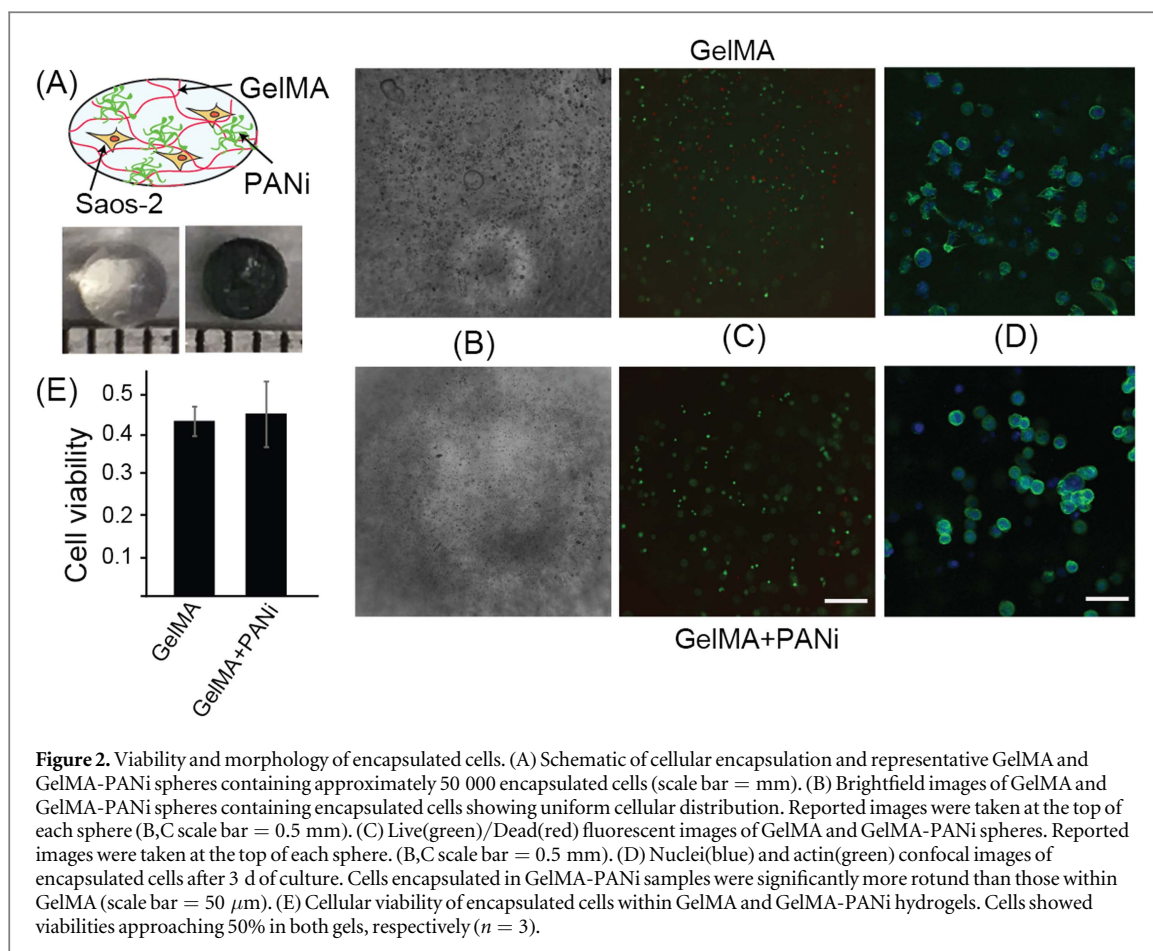


Figure 2. Viability and morphology of encapsulated cells. (A) Schematic of cellular encapsulation and representative GelMA and GelMA-PANi spheres containing approximately 50 000 encapsulated cells (scale bar = mm). (B) Brightfield images of GelMA and GelMA-PANi spheres containing encapsulated cells showing uniform cellular distribution. Reported images were taken at the top of each sphere (B,C scale bar = 0.5 mm). (C) Live(green)/Dead(red) fluorescent images of GelMA and GelMA-PANi spheres. Reported images were taken at the top of each sphere. (B,C scale bar = 0.5 mm). (D) Nuclei(blue) and actin(green) confocal images of encapsulated cells after 3 d of culture. Cells encapsulated in GelMA-PANi samples were significantly more rotund than those within GelMA (scale bar = 50 μ m). (E) Cellular viability of encapsulated cells within GelMA and GelMA-PANi hydrogels. Cells showed viabilities approaching 50% in both gels, respectively ($n = 3$).

homogenous, it was necessary to determine how the added PANi affected the electrical conductivity, modulus, and swelling ratio as compared to a GelMA only hydrogel. As expected, adding increasing concentrations of PANi to GelMA significantly increased the conductivity of the composite hydrogel (figure 1(E)), however the small dilution of GelMA macromer caused by increasing concentrations of PANi resulted in a drop in the hydrogel compressive moduli (figure 1(F)). Accordingly, a reduction in moduli was accompanied by an increasing swelling ratio as more GelMA was displaced by PANi (figure 1(G)), a correlation supported in previous work [34, 37].

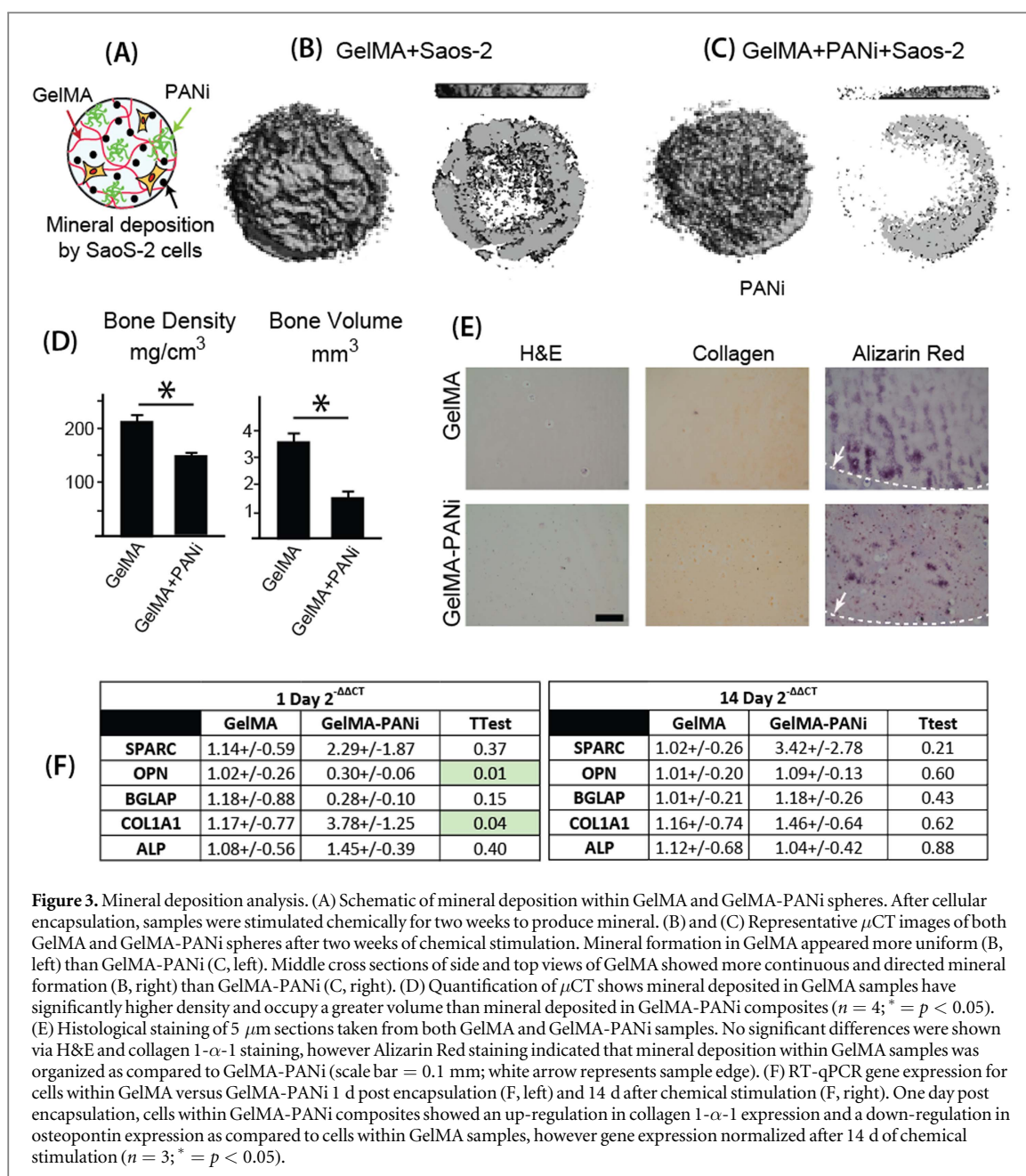
Cellular encapsulation

To determine the biocompatibility of GelMA-PANi composites, human osteosarcoma cells (Saos-2) were chosen to serve as a model line for the cellular encapsulation studies. GelMA and GelMA-PANi solutions pre-diluted with cells were crosslinked into spherical constructs approximately 2 mm in diameter (figure 2(A)). Twenty-four hours after encapsulation, brightfield images showed a homogenous distribution of cells throughout both types of hydrogels (figure 2(B)). Live/Dead analysis also showed a similar distribution of cells in both GelMA and GelMA-PANi hydrogels with viabilities between 40% and 50% respectively, a result consistent with other cellular encapsulation studies

(figures 2(C) and (E)) [34]. However, while both GelMA and GelMA-PANi hydrogels showed similar cellular distribution and viability, differences in cellular morphology could be observed (figure 2(D)). Confocal imaging of both the nuclei (blue) and cytoskeleton (green) of encapsulated cells after 3 d of culture showed that cells within a GelMA matrix displayed a spread morphology while those in GelMA-PANi samples had noticeably more spherical structures.

Mineral deposition

To demonstrate potential for bone tissue engineering applications, it was necessary to determine how the addition of conductive PANi would affect mineral deposition *in vitro* (figure 3(A)). Cells were encapsulated as previously described in either GelMA or GelMA-PANi hydrogels and chemically stimulated for two weeks with osteogenic media, after-which they were fixed and scanned for mineral accumulation. In both samples cell mineralization appeared to occur robustly at the periphery of the gels adjacent to the media interface and waned toward the center of the constructs (figures 3(B) and (C)). Despite this organization, mineral within the GelMA samples appeared more uniform and contiguous while mineral within the GelMA-PANi samples appeared disorganized. Quantification of μ CT imaging data further illustrated that GelMA-PANi samples were significantly less



dense and mineralized matrix occupied a significantly smaller volume fraction than that produced by samples composed of only GelMA (figure 3(D)). Non-cellular induced controls and non-induced cell-laden controls showed no mineralization, respectively, when analyzed via μ CT (data not shown).

Histological staining was performed on paraffin embedded GelMA and GelMA-PANi samples after two weeks of induction to evaluate differences in matrix deposition (figure 3(E)). Aside from PANi granules being visible in GelMA-PANi sections, no difference in morphology or collagen deposition was evident by H&E and collagen 1- α -1 stains, with cell lacunae being equally visible in both samples. Sections stained for mineral, however, did show differences with deposition in GelMA samples appearing organized and directional (figure 3(E), right panel top)

while deposition in GelMA-PANi samples appearing random and disordered (figure 3(E), right panel bottom). Furthermore, mineral deposition in GelMA samples occurred in a gradient pattern, with more mineral being deposited towards the hydrogel periphery and decreasing towards the center of the construct.

In order to determine the potential osteoconductive properties of GelMA-PANi hydrogels, we used RT-qPCR to assay expression of genes associated with osteoblastic matrix synthesis and mineralization in samples collected both 1 d after encapsulation and 14 d after culture (figure 3(F)). In samples collected 24 h after encapsulation, osteopontin expression was significantly down-regulated (1.02 to 0.30, $p = 0.01$) and collagen 1- α -1 expression was significantly up-regulated (1.17 to 3.78, $p = 0.04$) in GelMA-PANi samples relative to GelMA samples. However, after two weeks of culture,

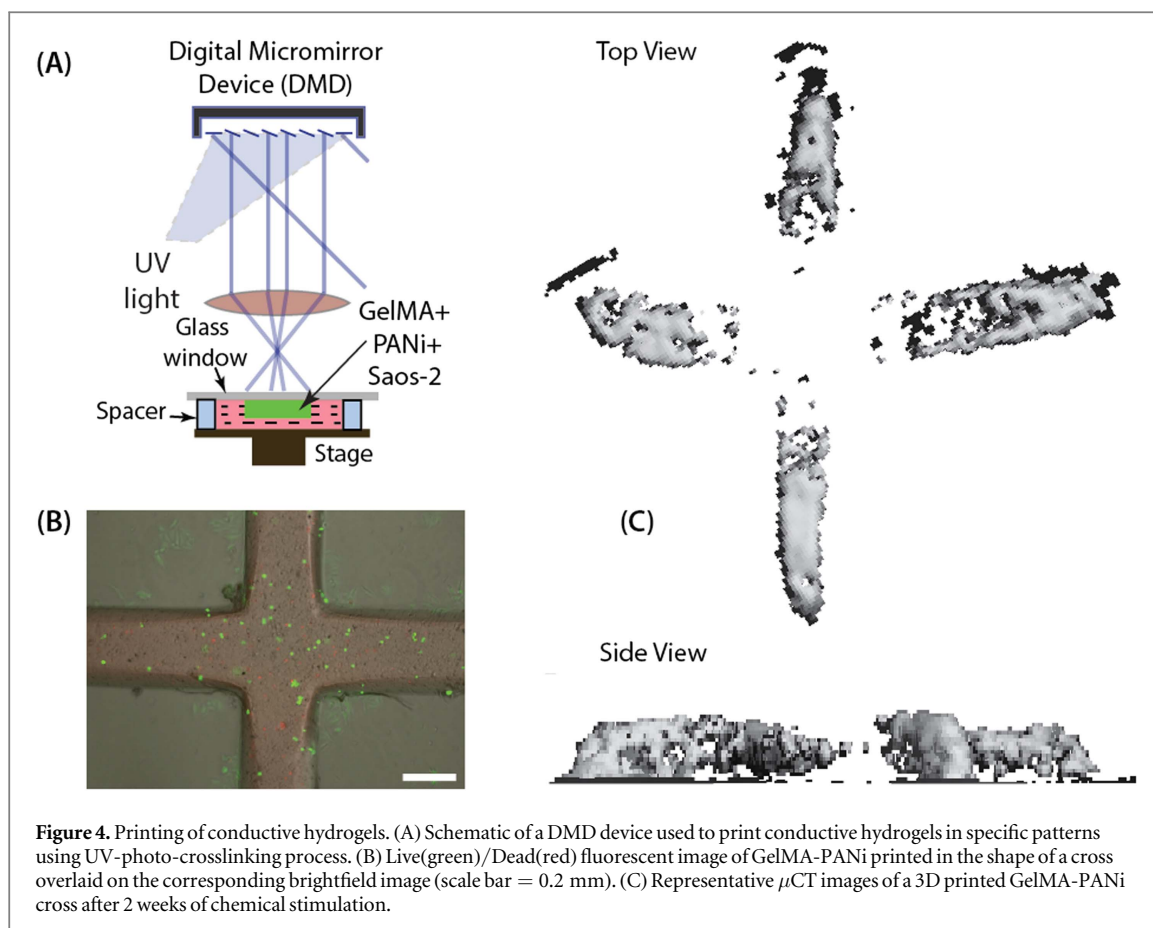


Figure 4. Printing of conductive hydrogels. (A) Schematic of a DMD device used to print conductive hydrogels in specific patterns using UV-photo-crosslinking process. (B) Live(green)/Dead(red) fluorescent image of GelMA-PANi printed in the shape of a cross overlaid on the corresponding brightfield image (scale bar = 0.2 mm). (C) Representative μ CT images of a 3D printed GelMA-PANi cross after 2 weeks of chemical stimulation.

gene expression in GelMA-PANi samples showed no significant differences relative to GelMA.

Printing of conductive hydrogels using digital stereolithography

Although a variety of conductive hydrogels have been developed, the poor mechanical properties of these materials do not allow for the fabrication of functional circuits. In this work, we used projection-based stereolithography to print GelMA-PANi lines at a micrometer resolution in order to establish a proof-of-concept that user-defined features could be printed using this material. A DMD (figure 4(A)) was used to print a 500 μ m thick cell-laden GelMA-PANi cross, with arms approximately 200 μ m wide. Live/Dead staining performed 24 h after printing showed high cellular viability in addition to an even cell distribution (figure 4(B)). Chemical induction for two weeks showed mineralization along the arms of the cross with no mineral formation in the center, presumably due to inherent diffusion limitations (figure 4(C)).

Discussion

The application of electrical signals in tissue engineering substitutes is under-explored as compared to more traditional biophysical and biochemical cues such as mechanical forces and growth factors. The limited

work in this field is most likely due to the challenges involved in developing new conductive biomaterials that provide a biomimetic 3D environment while still allowing for reliable charge transfer between living cells [38, 39]. This work develops a GelMA-PANi-cell composite that enables the encapsulated Saos-2 cells to be viable within a conductive 3D environment and deposit mineral within the matrix. Additionally, we demonstrate that this material can be printed into user-defined micro-geometries using a digital stereolithography method, a necessary first step in the successful integration of conductive hydrogels into functional tissue regenerating devices [40, 41].

We chose GelMA as our base hydrogel, as it has several advantages for use in bone tissue engineering. Not only is GelMA comprised of denatured collagen, the main organic component found in bone tissue [42], but it also retains bioactive cell-attachment sites within a hydrated mesh-like structure that allows for easy cell attachment and metabolic waste exchange with the surrounding media [43]. Additionally, GelMA can be processed into useful structures using UV-crosslinking, an easy-to-use processing method which has been shown to not cause lasting damage to encapsulated cells in short exposures [29]. Furthermore, due to the relative ease with which the hydrogel can be synthesized and cured, the addition of PANi and cells post processing make GelMA an optimal

medium for the creation of GelMA-PANi-Saos-2 composites.

For cell encapsulation experiments, GelMA was mixed with PANi and irradiated with UV light. The amount of PANi and exposure time was chosen to maximize the electrical conductivity within the composite hydrogel while at the same time maintaining the structural properties of GelMA. Based on the results (figures 1(E)–(G)), GelMA with 0.50 PANi provided maximal conductive properties and maintained a compressive modulus and swelling ratio suitable for cellular encapsulation. Furthermore, no significant difference in the viability of encapsulated Saos-2 cells in GelMA and GelMA containing 0.50 PANi was demonstrated (figure 2(E)), indicating that the PANi nanowires were not cytotoxic. The overall generally low viability of encapsulated Saos-2 cells within both types of hydrogels, however, could be attributed to diffusion limitations inherent in our comparably larger structures, an observation that was emphasized by the lack of mineralization in the diffusion limited center of the constructs (figures 3(B) and (C)). Accordingly, it has been shown that cells are required to be within 200–300 μm of a nutrient supply to function appropriately, indicating that future studies would need to address this obvious limitation.

The addition of PANi appeared to decrease the ability of encapsulated Saos-2 cells to spread (figure 2(D)), suggesting a possible interruption of cell attachment dynamics. Additionally, mineral deposition was significantly affected by the presence of PANi as both the density and volume of mineral deposited within the composite matrix was significantly lower than that deposited in GelMA (figure 3(D)). It has been shown recently that bone cells seeded onto softer matrices tend to deposit less mineral [44], a phenomena that lends an explanation to the reduced deposition in our softer GelMA-PANi composites. Furthermore, after 1 d of encapsulation, cells within GelMA-PANi hydrogels had an up-regulation of collagen 1- α -1 expression and a down-regulation of osteopontin relative to those within GelMA, indicating that the newly encapsulated cells in the composites were attempting to synthesize matrix for support rather than produce mineral. Alternatively, cells within GelMA hydrogels showed a more spread morphology (figure 2(D)) and produced mineral in a more ordered fashion (figures 3(C) and (E)), indicating that they were capable migrating readily through the gel.

Conductive GelMA-PANi composites were also amenable to stereolithographic printing. Specifically, by using a DMD printer it was possible to print lines of GelMA-PANi containing encapsulated cells in user-defined geometries, allowing for the potential fabrication of electro-active biological circuits. In future studies, cell-laden conductive hydrogels could be actively stimulated with external electrical cues, potentially serving as a novel way for the study of how active electrical signals affect cellular function.

Conclusion

In this work, we successfully demonstrated a novel method for incorporating a conductive polymer into a cell-laden, biomimetic hydrogel without compromising cell viability. Furthermore, we demonstrated that this conductive, cell-laden hydrogel is compatible with digital stereolithography, thereby allowing for the creation of spatially precise, user-defined structures. While there is much work that remains to be done to modulate cellular function, this research has developed an improved electro-conductive cell laden hydrogel for further investigation.

Acknowledgments

This work was partially supported by the National Science Foundation (NSF) (CMMI 1634997 and 1547095). This work was supported by the Soft Interfaces Integrative Graduate Education and Research Traineeship (IGERT) DMR-DGE- 1068780 at Syracuse University and funded by the National Science Foundation (NSF).

Author contribution

SS and PS wrote the manuscript; SS, PD, JH, and PS conceived and designed the experiments; SS and JH performed cell studies; PD and SV synthesized poly (aniline); DQ developed the resistance test-chip for conductive analysis; AR performed data analysis and synthesized GelMA macromer.

Statement of significance

Cell-laden GelMA-PANi hydrogel composites have a three-fold advantage over traditional platforms used for tissue engineering in that they are electrically conductive, support cellular viability and osteogenic mineralization, and are capable of being printed in user-defined microscale geometries.

ORCID iDs

Pranav Soman  <https://orcid.org/0000-0001-9456-0030>

References

- [1] Kloxin A M, Tibbitt M W and Anseth K S 2010 Synthesis of photodegradable hydrogels as dynamically tunable cell culture platforms *Nat. Protocols* **5** 1867–87
- [2] Lewis K J R and Anseth K S 2013 Hydrogel scaffolds to study cell biology in four dimensions *MRS Bull.* **38** 260–8
- [3] Tibbitt M W and Anseth K S 2009 Hydrogels as extracellular matrix mimics for 3D cell culture *Biotechnol. Bioeng.* **103** 655–63
- [4] Hwang S J *et al* 2011 The implications of the response of human mesenchymal stromal cells in three-dimensional

- culture to electrical stimulation for tissue regeneration *Tissue Eng. A* **18** 432–45
- [5] Shen F H *et al* 2013 Implications of adipose-derived stromal cells in a 3D culture system for osteogenic differentiation: an *in vitro* and *in vivo* investigation *Spine J.* **13** 32–43
- [6] Balint R, Cassidy N J and Cartmell S H 2014 Conductive polymers: towards a smart biomaterial for tissue engineering *Acta Biomater.* **10** 2341–53
- [7] Cao J, Man Y and Li L 2013 Electrical stimuli improve osteogenic differentiation mediated by aniline pentamer and PLGA nanocomposites *Biomed. Rep.* **1** 428–32
- [8] Dvir T *et al* 2011 Nanowired three-dimensional cardiac patches *Nat. Nanotechnol.* **6** 720–5
- [9] Ferris C J 2009 Conducting bio-materials based on gellan gum hydrogels *Soft Matter* **5** 3430–7
- [10] Gaharwar A K, Peppas N A and Khademhosseini A 2014 Nanocomposite hydrogels for biomedical applications *Biotechnol. Bioeng.* **111** 441–53
- [11] MacDonald R A, Voge C M, Kariolis M and Stegemann J P 2008 Carbon nanotubes increase the electrical conductivity of fibroblast-seeded collagen hydrogels *Acta Biomater.* **4** 1583–92
- [12] Ahadian S *et al* 2014 Hybrid hydrogels containing vertically aligned carbon nanotubes with anisotropic electrical conductivity for muscle myofiber fabrication *Sci. Rep.* **4** 4271
- [13] Lamberti F, Giullitti S, Giomo M and Elvassore N 2013 Biosensing with electroconductive biomimetic soft materials *J. Mater. Chem. B* **1** 5083–91
- [14] Shin S R *et al* 2013 Carbon-nanotube-embedded hydrogel sheets for engineering cardiac constructs and bioactuators *ACS Nano* **7** 2369–80
- [15] Guiseppi-Elie A 2010 Electroconductive hydrogels: synthesis, characterization and biomedical applications *Biomaterials* **31** 2701–16
- [16] Green R A *et al* 2012 Conductive hydrogels: mechanically robust hybrids for use as biomaterials *Macromol. Biosci.* **12** 494–501
- [17] Mawad D *et al* 2012 A single component conducting polymer hydrogel as a scaffold for tissue engineering *Adv. Funct. Mater.* **22** 2692–9
- [18] Harman D G *et al* 2015 Poly(3,4-ethylenedioxythiophene): dextran sulfate (PEDOT: DS)—a highly processable conductive organic biopolymer *Acta Biomater.* **14** 33–42
- [19] Ding H *et al* 2014 Biologically derived soft conducting hydrogels using heparin-doped polymer networks *ACS Nano* **8** 4348–57
- [20] Rivers T J, Hudson T W and Schmidt C E 2002 Synthesis of a novel, biodegradable electrically conducting polymer for biomedical applications *Adv. Funct. Mater.* **12** 33–7
- [21] Cao Y, Smith P and Heeger A 1989 Spectroscopic studies of polyaniline in solution and in spin-cast films *Synth. Met.* **32** 263–81
- [22] Zhang L and Wan M 2003 Self-assembly of polyaniline—from nanotubes to hollow microspheres *Adv. Funct. Mater.* **13** 815–20
- [23] Li M, Guo Y, Wei Y, MacDiarmid A G and Lelkes P I 2006 Electrospinning polyaniline-contained gelatin nanofibers for tissue engineering applications *Biomaterials* **27** 2705–15
- [24] Jang J, Ha J and Cho J 2007 Fabrication of water-dispersible polyaniline-poly(4-styrenesulfonate) nanoparticles for inkjet-printed chemical-sensor applications *Adv. Mater.* **19** 1772–5
- [25] Ngamna O, Morrin A, Killard A J, Moulton S E, Smyth M R and Wallace G G 2007 Inkjet printable polyaniline nanoformulations *Langmuir* **23** 8569–74
- [26] Kang E, Neoh K and Tan K 1998 Polyaniline: a polymer with many interesting intrinsic redox states *Prog. Polym. Sci.* **23** 277–324
- [27] Bidez P R, Li S, MacDiarmid A G, Venancio E C, Wei Y and Lelkes P I 2006 Polyaniline, an electroactive polymer, supports adhesion and proliferation of cardiac myoblasts *J. Biomater. Sci., Polym. Ed.* **17** 199–212
- [28] Humpolicek P, Kasparkova V, Saha P and Stejskal J 2012 Biocompatibility of polyaniline *Synth. Met.* **162** 722–7
- [29] Wu Y *et al* 2016 Fabrication of conductive gelatin methacrylate–polyaniline hydrogels *Acta Biomater.* **33** 122–30
- [30] Wu Y, Chen Y X, Yan J, Yang S, Dong P and Soman P 2015 Fabrication of conductive polyaniline hydrogel using porogen leaching and projection microstereolithography *J. Mater. Chem. B* **3** 5352–60
- [31] Li D and Kaner R B 2006 Shape and aggregation control of nanoparticles: not shaken, not stirred *J. Am. Chem. Soc.* **128** 968–75
- [32] Huang J and Kaner R B 2004 Nanofiber formation in the chemical polymerization of aniline: a mechanistic study *Angew. Chem.* **116** 5941–5
- [33] Chiou N-R and Epstein A J 2005 A simple approach to control the growth of polyaniline nanofibers *Synth. Met.* **153** 69–72
- [34] Sawyer S, Oest M, Margulies B and Soman P 2016 Behavior of encapsulated saos-2 cells within gelatin methacrylate hydrogels *J. Tissue Sci. Eng.* **7** 2
- [35] Murray E, Provvedini D, Curran D, Catherwood B, Sussman H and Manolagas S 1987 Characterization of a human osteoblastic osteosarcoma cell line (SAOS-2) with high bone alkaline phosphatase activity *J. Bone Mineral Res.* **2** 231–8
- [36] Bouxsein M L, Boyd S K, Christiansen B A, Guldberg R E, Jepsen K J and Müller R 2010 Guidelines for assessment of bone microstructure in rodents using micro-computed tomography *J. Bone Mineral Res.* **25** 1468–86
- [37] Chen Y X *et al* 2015 A novel suspended hydrogel membrane platform for cell culture *J. Nanotechnol. Eng. Med.* **6** 021002
- [38] Weaver J and Astumian R 1990 The response of living cells to very weak electric fields—the thermal noise limit *Science* **247** 459–62
- [39] Guarino V, Alvarez-Perez M A, Borriello A, Napolitano T and Ambrosio L 2013 Conductive PANi/PEGDA macroporous hydrogels for nerve regeneration *Adv. Healthcare Mater.* **2** 218–27
- [40] Jeong J-W, Shin G, Park S I, Yu K J, Xu L and Rogers J A 2015 Soft materials in neuroengineering for hard problems in neuroscience *Neuron* **86** 175–86
- [41] Green R A *et al* 2013 Living electrodes: tissue engineering the neural interface *Engineering in Medicine and Biology Society (EMBC), 2013 35th Annual Int. Conf. of the IEEE (Osaka, July 2013)* (Piscataway, NJ: IEEE) pp 6957–60
- [42] Robinson R A 1952 An electron-microscopic study of the crystalline inorganic component of bone and its relationship to the organic matrix *J. Bone Joint Surg. Am.* **34** 389–476
- [43] Yue K, Trujillo-de Santiago G, Alvarez M M, Tamayol A, Annabi N and Khademhosseini A 2015 Synthesis, properties, and biomedical applications of gelatin methacryloyl (GelMA) hydrogels *Biomaterials* **73** 254–71
- [44] Chatterjee K *et al* 2010 The effect of 3D hydrogel scaffold modulus on osteoblast differentiation and mineralization revealed by combinatorial screening *Biomaterials* **31** 5051–62